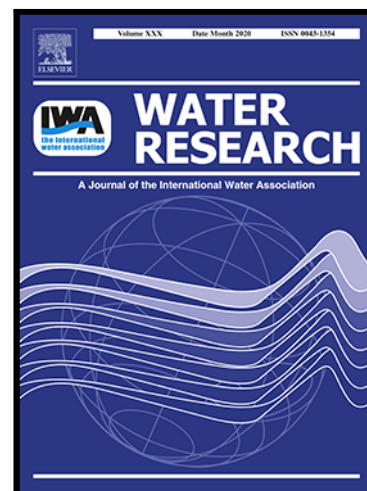


Journal Pre-proof

A quasi-Monte Carlo based flocculation model for fine-grained cohesive sediments in aquatic environments

Xiaoteng Shen , Mingze Lin , Yuliang Zhu , Ho Kyung Ha ,
Michael Fettweis , Tianfeng Hou , Erik A. Toorman ,
Jerome P.-Y. Maa , Jinfeng Zhang

PII: S0043-1354(21)00151-2
DOI: <https://doi.org/10.1016/j.watres.2021.116953>
Reference: WR 116953



To appear in: *Water Research*

Received date: 23 December 2020
Revised date: 17 February 2021
Accepted date: 18 February 2021

Please cite this article as: Xiaoteng Shen , Mingze Lin , Yuliang Zhu , Ho Kyung Ha , Michael Fettweis , Tianfeng Hou , Erik A. Toorman , Jerome P.-Y. Maa , Jinfeng Zhang , A quasi-Monte Carlo based flocculation model for fine-grained cohesive sediments in aquatic environments, *Water Research* (2021), doi: <https://doi.org/10.1016/j.watres.2021.116953>

This is a PDF file of an article that has undergone enhancements after acceptance, such as the addition of a cover page and metadata, and formatting for readability, but it is not yet the definitive version of record. This version will undergo additional copyediting, typesetting and review before it is published in its final form, but we are providing this version to give early visibility of the article. Please note that, during the production process, errors may be discovered which could affect the content, and all legal disclaimers that apply to the journal pertain.

© 2021 Published by Elsevier Ltd.

1 A quasi-Monte Carlo based flocculation model for fine-grained cohesive
2 sediments in aquatic environments

3 Xiaoteng Shen ^{1,2,3}, Mingze Lin ², Yuliang Zhu ^{1,2,3,*}, Ho Kyung Ha ⁴, Michael
4 Fettweis ⁵, Tianfeng Hou ^{6,7,8}, Erik A. Toorman ⁹, Jerome P.-Y. Maa ¹⁰, Jinfeng
5 Zhang ¹¹

6 ¹ Key Laboratory of Ministry of Education for Coastal Disaster and Protection, Hohai University,
7 Nanjing 210098, China

8 ² College of Harbour, Coastal and Offshore Engineering, Hohai University, Nanjing 210098, China

9 ³ Engineering Research Center of Ministry of Education for Dredging Technology, Hohai University,
10 Nanjing 210098, China

11 ⁴ Department of Ocean Sciences, Inha University, Incheon 22212, Republic of Korea

12 ⁵ Operational Directorate Natural Environment, Royal Belgian Institute of Natural Sciences, Rue Vautier
13 29, 1000 Brussels, Belgium

14 ⁶ Prediction Science Laboratory, RIKEN Cluster for Pioneering Research, Kobe, Japan

15 ⁷ Data Assimilation Research Team, RIKEN Center for Computational Science, Kobe, Japan

16 ⁸ RIKEN iTHEMS, Wako, Saitama 351-0198, Japan

17 ⁹ Hydraulics Laboratory, Department of Civil Engineering, KU Leuven, Kasteelpark Arenberg 40, B-3001
18 Leuven, Belgium

19 ¹⁰ Virginia Institute of Marine Science, College of William & Mary, Gloucester Point, VA 23062, United
20 States

21 ¹¹ State Key Laboratory of Hydraulic Engineering Simulation and Safety, Tianjin University, Tianjin
22 300072, China

23

* Corresponding author. Key Laboratory of Ministry of Education for Coastal Disaster and Protection, Hohai University, Nanjing 210098, China

E-mail addresses: zhuyl@hhu.edu.cn (Y. Zhu).

1 **Abstract**

2 The quasi-Monte Carlo (QMC) method was enhanced to solve the population balance model
3 (PBM) including aggregation and fragmentation processes for simulating the temporal evolutions
4 of characteristic sizes and floc size distributions (FSDs) of cohesive sediments. Ideal cases with
5 analytical solutions were firstly adopted to validate this QMC model to illustrate selected pure
6 aggregation, pure fragmentation, and combined aggregation and fragmentation systems. Two
7 available laboratory data sets, one with suspended kaolinite and the other with a mixture of
8 kaolinite and montmorillonite, were further used to monitor the FSDs of cohesive sediments in
9 controlled shear conditions. The model results show reasonable agreements with both analytical
10 solutions and laboratory experiments. Moreover, different QMC schemes were tested and
11 compared with the standard Monte Carlo scheme and a Latin Hypercube Sampling scheme to
12 optimize the model performance. It shows that all QMC schemes perform better in both accuracy
13 and time consumption than standard Monte Carlo scheme. In particular, compared with other
14 schemes, the QMC scheme using Halton sequence requires the least particle numbers in the
15 simulated system to reach reasonable accuracy. In the sensitivity tests, we also show that the
16 fractal dimension and the fragmentation distribution function have large impacts on the predicted
17 FSDs. This study indicates a great advance in employing QMC schemes to solve PBM for
18 simulating the flocculation of cohesive sediments.

19

20 **Key words:** Cohesive sediments; flocculation; quasi-Monte Carlo; population balance model;
21 floc size distribution

1 1. Introduction

2 Fine-grained cohesive sediments abound in open water systems such as estuaries, reservoirs,
3 and coastal waters. The transport of cohesive sediments has great impacts on bed morphology,
4 water quality, and estuarine circulations (Maggi, 2005; Edmonds and Slingerland, 2010; Geyer
5 and MacCready, 2014; Burchard et al., 2018). One significant characteristic of cohesive
6 suspended sediments is flocculation, which is the process where sediment particles go through
7 aggregation and fragmentation simultaneously to form clusters (flocs). Accurate modeling
8 flocculation of fine-grained sediments is still a challenge since the process is influenced by
9 physical (e.g., turbulence intensity and sediment concentration), biological (e.g., Extracellular
10 Polymeric Substances), and chemical (e.g., mineralogical composition, PH value, and salinity)
11 effects (Tolhurst et al., 1999; Winterwerp, 1998; Tran and Strom, 2019; Azhikodan and
12 Yokoyama, 2021; Fall et al., 2021).

13 Over the past decade, different kinds of flocculation models have been developed to track
14 the sediment particle quantities. The first is the simplified Lagrangian model (sometimes also
15 known as the floc growth model) developed by Winterwerp (1998) to track the evolution of a
16 characteristic size under shear-dominated environments. Later, the constant fractal dimension
17 (Maggi et al., 2007; Khelifa and Hill, 2006) and yield strength (Son and Hsu, 2009) in the
18 Winterwerp's model were enhanced as a function of floc size, and the breakage parameter was
19 connected with the Kolmogorov microscale (Kuprenas et al., 2018) to better address the effects
20 of suspended sediment concentration on flocculation. This low-cost single class model can be
21 easily adopted in real environments (e.g., Zhang et al., 2020); however, some properties of
22 flocculation such as the effects of differential settling and the variations of bi- or multi-peak
23 FSDs cannot be dealt with using the Winterwerp's model. The second flocculation model is the

1 population balance model (PBM), which is a transport model based on an integro-partial
2 differential equation that accounts for the number density of flocs with particular size at any
3 location and time in a system. Although PBM has been widely used in many fields (e.g., aerosol,
4 droplet, milling, and granulation), only few studies applied it to simulate FSDs for fine-grained
5 cohesive sediments in natural environments (e.g., Maggi et al., 2007; Lee et al., 2011; Shen and
6 Maa, 2015, 2016, 2017). Note that although the Winterwerp's model could be sometimes treated
7 as a one-class PBM, here it is classified separately since the model cannot track the bi- or multi-
8 peak FSDs. Most of the other flocculation models mainly focused on the details of forces
9 governing particle-particle interactions. For example, Zhang and Zhang (2011) extended the
10 Lattice Boltzmann Model by adding fluid-solid boundary using bounce-back method to simulate
11 the FSDs of cohesive sediments considering hydrodynamics and attractive van der Waals forces
12 during differential settling, and their model was later applied under shear conditions as well
13 (Zhang et al., 2013). In addition, Zhao et al. (2020) investigated the Stokes drag, lubrication,
14 cohesive, and direct contact forces between particles, which performed well in the transient stage
15 of flocculation in a conceptually simple and small cellular flow set-up. These models often
16 consume exorbitant memory and computational resources, which limits themselves on studying
17 large domains.

18 Among the above mentioned models, the population balance model (PBM) outperforms
19 other models for its advantages in the ability of tracking FSDs and describing various
20 flocculation mechanisms. Several numerical methods for solving PBM have been proposed,
21 including discretization methods (Kumar and Ramkrishna, 1996; Bertin et al., 2016; Kumar and
22 Kaur, 2016; Singh et al., 2019), moment methods (McGraw, 1997; Shen and Maa, 2015, 2016,
23 2017; Passalacqua et al., 2018; Li et al., 2019) and Monte Carlo (MC) methods (Khelifa and Hill,

1 2006; Xu et al, 2014; Lee et al., 2015; Das et al., 2020). The first approach, i.e., the discretization
2 method, converts the PBM to a series of ordinary differential equations by discretizing the
3 continuous number density function into several pivots to track the particle quantities (Singh et
4 al., 2019). The disadvantage of this method is the requirement of large computing resources to
5 obtain a desirable accuracy especially for cases with wide range of sizes (Shiea et al., 2020). The
6 second approach, the methods of moments, was developed as an approximated solution that
7 tracks the moments of the number density function and then reconstructs the number density
8 function. The process of reconstructing the FSDs from their moments, however, may cost
9 expensively in computing resource (Shen and Maa, 2015,2016; Li et al., 2019; Wang et al.,
10 2020). The third approach, the Monte Carlo (MC) methods, deals with physical processes such
11 as aggregation and fragmentation as discrete events by using probabilistic tools. With MC
12 methods, one can conveniently obtain the time evolution of particle systems by using an array
13 containing the particle size to represent a sample of the whole system and simulating the
14 particulate behaviors, which makes it suitable for extension to multivariate (e.g., size, density,
15 and biomass fraction) problems (Su et al., 2009; Zhao et al., 2011; Xu et al., 2014, Kotalczyk and
16 Kruis, 2017). This capability of easy extension for finding other physical properties is our main
17 motivation to use the MC method.

18 The MC methods for PBM can be classified into event-driven MC and time-driven MC by
19 time discretization. In event-driven MC (Garcia et al., 1987), a specific event (e.g., aggregation
20 and fragmentation) is first selected according to the probability that is proportional to the rate of
21 its occurrence. The time increment is calculated for each event during the simulation. In the
22 time-driven MC (Liffman, 1992), a specified time is first given less than the minimum time scale
23 of all the possible events, and then all possible occurring events proceed within this pre-specified

1 time. MC methods can also be divided into constant-volume MC and constant-number MC
2 according to the simulated volume. The former keeps the system in a constant volume and thus
3 changes the total number of particles but conserving the mass (Lin et al., 2002), while the latter
4 adjusts the volume to keep the particles number unchanged. With the constant-volume MC,
5 either the statistic error increases with time because of the reduction in particle number for
6 aggregation events, or the computational cost increases due to the increasing particle number for
7 fragmentation events. To balance the simulation efficiency and accuracy, the constant-number
8 MC was developed to keep the particle number unchanged during the simulation by continuously
9 adjusting the sampling volume (Tang and Matsoukas, 1997; Smith and Matsoukas, 1998).

10 The MC methods have rarely been applied to solve PBM for simulating the time evolution
11 of FSDs for suspended sediments flocculation, except for some early studies by Khelifa et al.
12 (2005, 2006). Although the MC methods have their superior discrete nature, the convergence rate
13 of standard MC method can often be very slow, which costs more computational resources and
14 time, especially for multivariate and high-dimensional problems (Caflisch, 1998; Wang and
15 Sloan, 2011; Singhee and Rutenbar, 2010; Dick et al., 2013). Thus, a quasi-Monte Carlo (QMC)
16 method was later developed by using quasi-random numbers (namely the low-discrepancy
17 sequences) instead of standard MC's pseudorandom numbers (Radović et al., 1996; Sobol, 1998;
18 Hou et al., 2019) to improve the efficiency and accuracy of standard MC. In this way, the QMC
19 scheme for solving PBM has an optimal combination of high accuracy and efficiency.

20 The objective of this study is to simulate the temporal evolution of FSDs and characteristic
21 sizes (e.g., mean size and median size) of fine-grained suspended sediments including
22 aggregation and fragmentation using a modified quasi-Monte Carlo based PBM. In order to
23 check the effectiveness of the model, data from (1) three analytical solutions given by Scott

1 (1968), Ziff and McGrady (1985) and McCoy and Madras (2003) including pure aggregation,
 2 pure fragmentation, and combined aggregation and fragmentation systems, respectively, and (2)
 3 two laboratory experimental results from Tran and Strom (2017) and Maggi et al. (2002, 2007)
 4 are used for validations. Furthermore, the effectivity and efficiency of different QMC schemes
 5 are tested and compared with standard MC scheme to find the optimal model performance. The
 6 sensitivities on selected parameters are also discussed in order to investigate the model behavior.

7 This paper is organized as follows. Section 2.1 reviews the PBM model and explains the
 8 selection of inner functions in PBM. Section 2.2 presents the QMC schemes and describes the
 9 flocculation model. The model is thus calibrated and validated in section 3, with three analytical
 10 solutions and two laboratory experimental data sets. In the following, the discussion and
 11 conclusions are delivered in Section 4 and Section 5 respectively.

12 2. Flocculation model

13 2.1 Population balance model and sediment flocculation dynamics

14 The PBM model, neglecting the advection, diffusion and settling terms, is used to
 15 characterize aggregation and fragmentation dynamics to model the time evolutions of number
 16 density of flocs with size D . The size-based PBM in a continuous form can be written as
 17 (Marchisio et al., 2003b; Kariwala et al., 2012; Shen and Maa, 2016):

$$\begin{aligned}
 \frac{\partial n(D, t)}{\partial t} = & \frac{D^2}{2} \int_0^D \frac{\beta \left((D^3 - \eta^3)^{\frac{1}{3}}, \eta \right) \cdot \alpha \left((D^3 - \eta^3)^{\frac{1}{3}}, \eta \right)}{(D^3 - \eta^3)^{\frac{2}{3}}} \cdot n \left((D^3 - \eta^3)^{\frac{1}{3}}, t \right) \cdot n(\eta, t) d\eta \\
 & - n(D, t) \int_0^\infty \beta(D, \eta) \cdot \alpha(D, \eta) \cdot n(\eta, t) d\eta + \int_L^\infty a(\eta) \cdot b(D|\eta) \cdot n(\eta, t) d\eta \\
 & - a(D) \cdot n(D, t)
 \end{aligned}$$

$$1 \quad \quad \quad (1)$$

2 where $n(D, t)$ is the number density function of particles with size D at time t , $\beta(D, \eta)$ is the
3 collision frequency for two particles of size D and η that collide to form a particle with size
4 $(D^3 + \eta^3)^{1/3}$, $\alpha(D, \eta)$ is the collision efficiency, $a(D)$ is the fragmentation frequency for
5 particles with size D , and $b(D|\eta)$ is the fragmentation distribution function that includes
6 information on the daughter particles produced by fragmentation. The first term on the right-
7 hand side of Eq. 1 is the birth rate of flocs with size D due to aggregation of smaller particles, the
8 second term is the death rate of flocs with size D due to aggregation with other particles, the
9 third term is the birth rate of flocs with size D due to fragmentation of bigger flocs with size η ,
10 and the last term is the death rate of flocs with size D due to their own fragmentation.

11 The collision efficiency α describes the probability of successful aggregation after collision
12 between flocs. It is often used in the form of a calibration parameter (e.g., Mietta et al., 2008;
13 Shen and Maa, 2015; Verney et al., 2011). The collision frequency β between sediment particles
14 with size D_i and D_j in natural environments consists of three mechanisms: Brownian motion,
15 differential settling, and turbulent shear. These terms can be written as (Smoluchowski, 1917;
16 Maggi, 2005; Shen and Maa 2015)

$$17 \quad \beta_{i,j} = \beta_{i,j}^{(BM)} + \beta_{i,j}^{(DS)} + \beta_{i,j}^{(TS)} \quad (2)$$

18 in which

$$19 \quad \text{Brownian motion} \quad \beta_{i,j}^{(BM)} = \frac{2}{3} \frac{kT}{\mu} \frac{(D_i + D_j)^2}{D_i D_j} \quad (3)$$

$$20 \quad \text{Differential settling} \quad \beta_{i,j}^{(DS)} = \frac{\pi}{4} (D_i + D_j)^2 |\omega_{s,i} - \omega_{s,j}| \quad (4)$$

$$21 \quad \text{Turbulent shear} \quad \beta_{i,j}^{(TS)} = \frac{G}{6} (D_i + D_j)^3 \quad (5)$$

1 where K is the Boltzmann constant, T is the absolute temperature, μ is the dynamic viscosity of
2 the fluid, $\omega_{s,i}$ and $\omega_{s,j}$ are the settling velocities of particles i and j , and G is the shear rate.
3 Although Brownian motion is commonly known as a negligible factor in estuaries region
4 (McCave, 1984; Winterwerp, 1998; Shen et al., 2018b), it is considered in this study for a
5 complete expression.

6 The fragmentation frequency function $a(D)$ accounts for the disruption of flocs by stress
7 produced by fluid shear and collision between flocs. The relative importance of these two
8 influences are still debatable and not well understood (Khelifa and Hill, 2006; Shen and Maa,
9 2015). Models for floc fragmentation often employ complicated functions with fitting parameters
10 (Winterwerp, 1998, 1999; Maggi et al., 2007; Shen and Maa, 2015, 2017). It is important to note
11 that the probability of fragmentation of particles can be easily related to the floc size (Khelifa
12 and Hill, 2006). A common kinematic approach regarding floc breakage defines a maximal floc
13 size D_{\max} instead of specifying the mechanism for fragmentation, which assumes that overlarge
14 (i.e., larger than D_{\max}) flocs always tend to break into fragments. The fragmentation distribution
15 function $b(D|\eta)$ describes the number and size of daughter flocs after fragmentation. The
16 assumptions used in this function are the discrete (e.g., binary breakup with mass ratio 1:1 or
17 ternary breakup with mass ratio 1:1:2, see Spicer and Pratsinis, 1996; Shen, 2015) and the
18 continuous form (e.g., Gaussian distribution).

19

20 2.2 Monte Carlo and Quasi-Monte Carlo

21 In this study, the constant-number MC method is applied in order to keep constant statistic
22 accuracy over the simulation (Lin et al., 2002). As described in Fig. 1, random number
23 generation (RNG) is the first step to produce a series of random numbers. The input parameters

1 are the particles number (N), the maximum size (D_{\max}) of flocs, the turbulent energy dissipation
 2 rate, and the densities of solid particles (ρ_s) and of the fluid (ρ_w). The initial size distribution
 3 (ISD), fractal dimension (nf), and the fragmentation distribution function were selected before
 4 the events module. The initial particle array is filled randomly with a specific size distribution
 5 (e.g., Gaussian distribution and uniform distribution). The fractal dimension (nf) of flocs are
 6 given by (Maggi et al., 2007)

$$7 \quad nf = 3 \cdot \left(\frac{D_f}{D_p}\right)^\delta \quad (6)$$

8 where D_p is the primary particle size, and $\delta = -0.1$ is used as suggested by Maggi et al. (2005).
 9 The floc size, D_f , is converted to component particle numbers, N_f , to better track and conserve the
 10 mass, similar as proposed by Maggi (2005) and Khelifa and Hill (2006):

$$11 \quad N_f = \left(\frac{D_f}{D_p}\right)^{nf} \quad (7)$$

12 The next step is choosing the aggregation or fragmentation events. Since little is known
 13 about the occurrence rate of the fragmentation, the following probability P_{frag} of floc breakage
 14 based on the number of overlarge flocs (larger than D_{\max}) is used as suggested by Khelifa and
 15 Hill (2006):

$$16 \quad P_{\text{frag}} = \begin{cases} 0, & n_b = 0 \\ 0.5, & n_b = 1 \\ 1, & n_b > 1 \end{cases} \quad (8)$$

17 where n_b is the number of overlarge flocs. The aggregation probability is $P_{\text{agg}} = 1 - P_{\text{frag}}$ since
 18 the null event is not considered in the simulation. A random number r_1 is taken from the random
 19 number series which is produced before simulating. The aggregation event is selected if $P_{\text{frag}} < r_1$,
 20 otherwise the fragmentation event is selected.

1 The acceptance-rejection (AR) method is applied in the implementation of each selected
 2 event. Two random particles i and j are selected and their aggregation kernel $A_{ij} = \alpha_{ij} \cdot \beta_{ij}$ is
 3 calculated by Eqs. 2~5 with a constant $\alpha = C_1$ for the aggregation event. Here, the collision
 4 efficiency α is set as unity, which raises the flocculation rate while reasonably maintaining the
 5 feature of floc size distributions (Khelifa and Hill, 2006). This selection based on the assumption
 6 that α does not significantly depend on floc properties (e.g., size, shape, and biomass fraction) in
 7 our cases; nevertheless, the α shall be more challenging in QMC models if the biomass fraction
 8 is highlighted in natural waters (Kiørboe et al., 1990; Lai et al., 2018). A random number r_2 is
 9 taken from the random number series produced before the simulation. The pair of selected
 10 particles i and j would aggregate to a floc containing $N_i + N_j$ component particles (Fig. 1) if the
 11 aggregation kernel A_{ij} satisfies the following condition (Khelifa and Hill, 2006; Zhao and Zheng,
 12 2013; Kotalczyk and Kruis, 2017):

$$13 \quad r_2 \leq A_{ij}/A_{\max} \quad (9)$$

14 where A_{\max} is the maximum of the aggregation kernel over all possible pairs. After a successful
 15 aggregation, the new formed floc is stored in the position of particle i . Then the position vacated
 16 by particle j is occupied by a duplicated particle of randomly selected particle k . If Eq. 9 is not
 17 satisfied, a new pair of particles is selected and the procedure is repeated until a pair of particles
 18 successfully aggregates.

19 Note that the calculation of the maximum aggregation kernel A_{\max} requests a double looping
 20 over all pairs of particles in each step, which computes expensively $N(N-1)/2$ times for every try.
 21 A simple constant maximum kernel may be used to reduce the calculation time as proposed by
 22 Smith and Matsoukas (1998), which is computationally feasible but not efficient in practical
 23 application for cohesive sediments. Kruis et al. (2000) introduced a so-called bookkeeping

1 strategy that calculates the aggregation kernels of all pairs of particles first and only updates the
 2 kernel of which particle size is changed after each event. Eibeck and Wagner (2001) and Xu
 3 (2014) proposed a differential weight MC (DWMC) which used the majorant of the aggregation
 4 kernel to calculate the A_{\max} by a single looping over all particle pairs instead of double looping.
 5 Although both the bookkeeping strategy and DWMC cost less CPU time than a traditional
 6 double looping strategy, they still consume much time when the particle number N is large.
 7 Khelifa and Hill (2006) proposed an automatically adjusted correction factor C_F to estimate the
 8 A_{\max} by multiplying with the kernel of the mean size of flocs, which is validated with in-situ data
 9 of FSDs of cohesive sediments. Thus, the A_{\max} is estimated as

$$10 \quad A_{\max} = C_F A_{\text{mean}} \quad (10)$$

11 with

$$12 \quad C_F = \frac{4n_a}{n_r + n_a} \quad (11)$$

13 where A_{mean} is the aggregation kernel of flocs with mean size, and n_a and n_r are the number of
 14 accepted and rejected tries respectively during each aggregation event. It is critical to note that
 15 the linear variation of C_F tends to remain the ratio $n_a : n_r$ close to one and the calculation of A_{\max}
 16 in Eq. 10 implies an assumption that $A_{\max} \sim 2A_{\text{mean}}$ in the simulation.

17 In the case of a fragmentation event, a particle i is selected randomly from the array. The
 18 acceptance-rejection (AR) method is also used to test the breakup probability with $B_i = N_{fi} / N_{\max}$.
 19 A random number r_3 from the pre-produced series is taken. If $B_i \geq r_3$, the particle i breaks into
 20 daughter flocs. Taking binary fragmentation as an example (Fig. 1), a random number r_4 is taken
 21 from the series produced already. The particle i breaks into two fragments i' with $r_4 \cdot N_{fi}$
 22 component particles and i'' with $(1-r_4) \cdot N_{fi}$ component particles as follows:

$$\begin{cases} N_{fi'} = r_4 N_{fi} \\ N_{fi''} = (1 - r_4) N_{fi} \end{cases} \quad (12)$$

1

2 The daughter particle i' is placed in the position of particle i , while the particle i'' replaces a
3 particle in the system stochastically.

4 After each step of aggregation or fragmentation, those key variables such as nf , D_f , N_f of
5 changed particles will be updated. The simulation will be terminated when equilibrium has been
6 reached. The FSDs and the characteristic sizes can be directly computed from the particle array.

7 Although the standard Monte Carlo method using pseudorandom numbers shows an
8 advantage of discrete nature for solving PBM, it needs to be enhanced due to the huge
9 computation cost. Thus, quasi-Monte Carlo schemes are developed to improve the performance
10 of standard MC by substituting the pseudorandom numbers by quasi-number sequences
11 (Singhee and Rutenbar, 2010; Dick et al., 2013; Hou et al., 2019), namely the deterministic
12 low-discrepancy sequences, which show more uniformity in distribution. Two different quasi-
13 number sequences, the Halton sequence (Halton, 1960) and the Sobol' sequence (Sobol, 1967),
14 will be used in this numerical study. The Halton sequence is the first class of low-discrepancy
15 sequences constructed in 1960 by Halton, which was frequently selected to substitute
16 pseudorandom numbers in standard MC due to its good performance and simplicity (Wang and
17 Hickernell, 2000; Hess and Polak, 2003; Mascagni and Chi., 2004; Chi et al., 2005). The Sobol'
18 sequence belongs to a new class of sequences called LP_τ -sequences introduced in 1966, which
19 has additional uniformity properties and can be computed in a "superfast" way using logical
20 operations (Sobol, 1998; Burhenne et al., 2011).

21 Besides, the Latin Hypercube Sampling (LHS) sequence (McKay and Beckman, 1979) as a
22 classic low-discrepancy sequence is also tested. The LHS is suggested as a particular kind of
23 stratified sampling to improve the efficiency of different sampling methods and used to be an

1 alternative of standard MC numbers in many research fields such as finite element analysis,
 2 structural reliability, and statistical circuit analysis (e.g., Keramat and Kielbasa, 1997; Olsson et
 3 al., 2002, 2003; Singhee and Rutenbar, 2010).

4 In order to better assess the uniformity of different sequences, 1000 points generated by
 5 each of four random number sequences are scatter-plotted in Fig. 2. One can easily see that the
 6 pseudorandom number and LHS sequences has more gaps and clumps than the other two
 7 sequences. In other words, the Halton sequence and the Sobol' sequence distribute visually more
 8 uniform than the others. For the purpose of qualifying the uniformity of these sequences, we
 9 define an area ratio index for the scatter-plot (Fig. 2) as

$$10 \quad r_a = \frac{A_{\text{seq}}}{A_{\text{all}}} \quad (13)$$

11 where A_{seq} is the summed area in the image taken by all the markers of each points sequence, A_{all}
 12 is the whole area enclosed by the coordinates $x = 0$ to 1 and $y = 0$ to 1 (in this case). The value of
 13 index r_a is between 0 to 1, and $r_a = 1$ denotes that the sequence is uniformly distributed. In this
 14 study, the radius of each marker is empirically set to 20 pounds, and thus A_{seq} can be calculated
 15 using image processing tools. As shown in Fig. 2, the area ratio index r_a shows that not only the
 16 pseudorandom number series is less geometrically uniform than the low-discrepancy series but
 17 the uniformity of the Sobol' and Halton sequences are also of a higher level than others. The
 18 efficiency and accuracy of all four sequences-based MC method to solve PBM will be discussed
 19 later in Section 4.1.

20

21 3. Case study

22 In the following cases, all simulations were performed with $N = 30,000$ particles, which will
 23 be discussed in more details in section 4. Simulations were run for 5×10^5 MC steps.

1 Temperature and the dynamic viscosity of the water were kept constant at 20 °C and 0.001 Pa·s.
 2 The density of the water and component particles were set to 1020 kg/m³ and 2650 kg/m³
 3 respectively.

4

5 3.1 Comparison with selected analytical solutions

6 Case I: Pure aggregation

7 Based on the assumption that aggregation between particles is totally at random, a constant
 8 aggregation kernel is considered, which indicates that each pair of selected particles (i, j) is
 9 always aggregated after collision. With the simple assumption of Eq. 14,

$$10 \quad \beta_{i,j} = \beta_0 \quad (14)$$

11 the analytical solution of the PSD for this case is given by Scott (1968) as

$$12 \quad n(D, t) = \frac{12N_0D^2}{v_0(T_a+2)^2} e^{-\frac{2D^3}{v_0(T_a+2)}} \quad (15)$$

13 The initial particle distribution is specified as $T_a = 0$ in Eq. 16

$$14 \quad n(D) = \frac{3N_0}{v_0} D^2 e^{-\frac{D^3}{v_0}} \quad (16)$$

15 in which N_0 is the initial total number of particles per unit volume (in units of m⁻³), v_0 is the mean
 16 volume of the particles at the beginning (in units of m⁻³), and $T_a = N_0\beta_0 t$ is dimensionless time.

17 Since the constant-number MC and the event-driven MC were applied in this study, the
 18 inter-event time need to be computed while running the model. Smith and Matsoukas (1998)
 19 gave the time increment of aggregation as

$$20 \quad \Delta t_\kappa = \frac{2\tau_c}{\langle \beta_{ij} \rangle} \cdot \frac{1}{N} \cdot \left(\frac{N}{N-1} \right)^\kappa \quad (17)$$

21 with

$$22 \quad \tau_c = 1/\beta_c C_0 \quad (18)$$

1 where Δt_κ is the time increment (in units of s), κ is the counter of successful aggregation events,
 2 τ_c is the characteristic aggregation time, β_c is the dimensional part of the aggregation kernel (in
 3 units of m^3/s) which equals to β_0 in this case, and C_0 is total particle number concentration at the
 4 beginning. In addition, $\langle \beta_{ij} \rangle$ is the ensemble average kernel, which can be written as a discrete
 5 form, namely

$$6 \quad \langle \beta_{ij} \rangle = \frac{\sum_i^N \sum_{j \neq i}^N \beta_{ij}}{N(N-1)} \quad (19)$$

7 All of the constants are selected the same as those of earlier researches on the purpose of
 8 comparing the model results with these earlier studies. For instance, $C_0 = N_0 = 1$, $\nu_0 = 1$, and $\langle \beta_{ij} \rangle$
 9 $= \beta_c = \beta_0 = 1$ are used in this study to match those of Shen and Maa (2016). Note that the
 10 analytical solution is a general formulation, the units of those parameter such as D , N_0 and ν_0 in
 11 Eq. 15~16 are not important and only require consistency. The cumulative time t can be derived
 12 from Eq. 17 as

$$13 \quad t = \sum_{\kappa=1}^{\kappa} \Delta t_\kappa = 2 \left(\left(\frac{N}{N-1} \right)^\kappa - 1 \right) \quad (20)$$

14 Since the initial particle size distribution cannot be fitted perfectly with the discrete
 15 character of Monte Carlo method, the initial FSD calculated by analytical solution is divided into
 16 1500 size classes and fitted approximately with $N = 30,000$ particles. In order to simplify the
 17 computation, the particle size at the peak concentration at $t = 0$ is selected as the primary particle
 18 size, i.e., $D_p = 0.87$ (in arbitrary length units), as inputs of the model in this case.

19 The predicted and analytical FSDs fit well with at $t = 0, 10, 20, 50, 100, 200$, and 300 s (Fig.
 20 3). One can easily calculate the arithmetic mean size (mean of number-based FSD) of the
 21 analytical solution given as (Shen and Maa, 2016)

$$22 \quad D_{mn} = \frac{\int_0^\infty Dn(D,t)dD}{\int_0^\infty n(D,t)dD} \quad (21)$$

1 by integral calculation. The simulated mean size also matches well with those given by analytical
 2 solution of the FSD (Fig.3).

3 To better evaluate the progress of aggregation of a system, Marchisio et al. (2003a), gave an
 4 index $I_a = 1 - m_0(t)/m_0(0)$ to show the degree of aggregation, and Scott (1968) gave the analytical
 5 solution for all the moments, as

$$6 \quad m_k(t) = m_k(t=0) \cdot \left(\frac{2}{2+N_0\beta_0 t} \right)^{1-\frac{k}{3}} \quad (22)$$

7 where $m_k(t)$ is the k th moments of FSD at time t . In this case, $m_0(0) = \int_0^\infty n(D,0)dD = 1$. Here $I_a =$
 8 0 indicating no aggregation, and $I_a = 1$ denotes aggregation progresses in full pace. The relative
 9 error for mean size between simulated and the analytical result is less than 13% even at $t = 1000$
 10 s, and the calculated $I_a = 99.8\%$ for the system at that time indicates that aggregation is still in
 11 progress with full pace.

13 Case II: Pure fragmentation

14 We consider the population balance model for a power breakup kernel as

$$15 \quad a(D) = a_0 D^3 \quad (23)$$

16 where $a_0 = 1$ together with a uniform fragmentation distribution given by Su et al. (2008) as

$$17 \quad b(D|\lambda) = \frac{(6D^2)}{\lambda^3}, \quad 0 < D < \lambda \quad (24)$$

18 Limited by the nature of discretion of MC method, the chosen floc will break into two classes j
 19 and k . Each of that includes two daughter flocs of the same size. The size of daughter flocs is
 20 decided by a random number r_4 as

$$21 \quad \begin{cases} N_{fj1} = N_{fj2} = r_4 N_{fi} \\ N_{fk1} = N_{fk2} = N_{fi}(1 - 2r_4)/2 \end{cases} \quad (25)$$

1 The time interval Δt_κ of the counter of successful fragmentation events κ , is given by Tang
 2 and Matsoukas (1997) as

$$3 \quad \Delta t_\kappa = \frac{1}{\langle K_i \rangle} \cdot \left(1 - \frac{M_\kappa}{M_{\kappa-1}} \right) \quad (26)$$

4 where $\langle K_i \rangle = \sum_i^N K_i / N$ is the mean fragmentation rate, and $M_{\kappa-1}$ and M_κ are the average mass
 5 before and after the κ fragmentation event. In order to reduce the computational resource, the
 6 average mass is estimated by the mass of the particle with average size.

7 The analytical solution of the FSD was given by Ziff and McGrady (1985) with the power
 8 initial distribution (Eq. 16) for this pure fragmentation case as follows

$$9 \quad n(D, t) = \frac{3D^2 N_0}{v_0} (1 + a_0 v_0 t)^2 e^{-\frac{D^3}{v_0} (1 + a_0 v_0 t)} \quad (27)$$

10 In this case, we considered $N_0 = 1$ and $v_0 = 1$ following Shen and Maa (2016). It can be seen
 11 in Fig. 4 that all of FSDs at selected time and mean size obtained by model coincide with the
 12 analytical solution. The mean size and the peak size decrease quickly with the progression of
 13 fragmentation in the first ten seconds and the rate of reduction is slowing down with time. In
 14 addition, the maximum relative errors of mean size between analytical solution and the MC
 15 model at selected time is less than 9%.

16 One should be aware that Case I and Case II are rarely possible for cohesive sediments in
 17 natural waters, since aggregation and fragmentation are often co-existing. Flocs do not unlimited
 18 grow or decay. But these two cases were simulated to show that the QMC model works well
 19 under pure aggregation and pure fragmentation conditions, as pre-steps to validate true cohesive
 20 sediment cases. The results of Case I and Case II illustrate that the constant-number QMC
 21 scheme, compared to the previous constant-volume QMC scheme, maintains stable statistical
 22 accuracy when particles aggregate and requires reasonable memory when particles break up.

23

1 Case III: Combined aggregation and fragmentation

2 For the combined aggregation and fragmentation case, McCoy and Madras (2003) obtained
 3 a solution of the FSD for a constant aggregation kernel (Eq. 14 with a constant β_0), a power
 4 breakage kernel (Eq. 23 with a constant a_0), a uniform fragmentation distribution function (Eq.
 5 24~25), and an exponent initial distribution (Eq. 16) with the analytical FSD given by

$$6 \quad n(D, t) = \frac{3N_0^2}{v_0} D^2 [\Phi(T_a)]^2 e^{-\frac{N_0}{v_0} D^3 \Phi(T_a)} \quad (28)$$

7 and the total number fraction at T_a follows

$$8 \quad \Phi(T_a) = \frac{\Phi(\infty) \cdot [1 + \Phi(\infty) \cdot \tanh(\Phi(\infty) \cdot \frac{T_a}{2})]}{\Phi(\infty) + \tanh(\Phi(\infty) \cdot \frac{T_a}{2})} \quad (29)$$

9 where $\Phi(\infty) = (2a_0 v_0 N_0 / \beta_0)^{0.5} / N_0$.

10 The time increment of a chosen event is calculated by Eq. 17 and Eq. 26. Fig. 5 presents the
 11 comparison of FSD and the mean size between the analytical solution and the model with those
 12 constants selected as $\beta_0 = 100$ in Eq. 14, $a_0 = 1 \times 10^{-6}$ in Eq. 23, and $N_0 = 1$, $v_0 = 100$ in Eq. 26
 13 (Shen and Maa, 2016). The system reached an equilibrium state under the selected conditions
 14 after around fifty seconds. It can be observed that the model results at all time match quite well
 15 with the analytical solution. The aggregation process plays a leading role in the first 10 seconds
 16 and the mean size increases quickly. Then the fragmentation processes start to occur more
 17 frequently and the system reaches a steady state.

18

19 3.2 Comparison with experimental data

20 Case IV: Tran's mixing chamber experiment

1 Tran and Strom (2017) conducted a laboratory experiment to explore the interaction
2 between clays and silts under turbulent shear conditions. The experiments were carried out in a
3 mixing chamber of $27.5 \times 27.5 \times 25 \text{ cm}^3$, in which a variable speed paddle mixer was set to
4 generate different magnitudes of turbulent shear. The pure clay sample consisted of a mixture of
5 80% kaolinite and 20% montmorillonite to mimic estuarine mud (Keyvani and Strom, 2014) and
6 the concentration was maintained constant at 100 mg/L. Floc images were recorded by a camera
7 system with a LED in a waterproofed housing placed inside the mixing tank. The field of camera
8 view was $2.4 \times 1.4 \text{ mm}^2$ with an image resolution of $1.3 \text{ }\mu\text{m}/\text{pixel}$. The pure clay suspension was
9 sonicated for 15 min to break down large clay aggregates and to obtain an average initial size
10 distribution around $5 \text{ }\mu\text{m}$. Then the suspension was introduced to clearwater fluid and mixed at G
11 $= 50 \text{ s}^{-1}$ and $G = 95 \text{ s}^{-1}$ respectively. The initial particle distribution obeys a Gaussian distribution
12 with mean D_p and standard deviation $D_p/3$. The maximum floc size was selected as the maximum
13 value between the Kolmogorov scale and the 95th percentile D_{95} . Besides, the quantity and sizes
14 of daughter flocs due to breakage of bigger flocs are logically and simply described by binary
15 fragmentation at current stage (e.g., Khelifa and Hill, 2006; Lee and Molz, 2014; Mietta et al.,
16 2011; Verney et al., 2011). Other aggregation and breakage fitting parameters are given in Table.
17 1.

18 It can be observed in Fig. 6 (a) and (b) that the aggregation dominates in the first $2 \times 10^5 \text{ MC}$
19 steps. But the particle size grows at a low speed within the first 10^5 MC steps since the floc size
20 still remains in the small level. The rate of increasing of floc size is higher between 1×10^5 and
21 $2 \times 10^5 \text{ MC}$ steps and larger flocs start to appear. After $2 \times 10^5 \text{ MC}$ steps, the fragmentation rate
22 gradually rises and the slope of the curve of median floc size is getting flatter. The system
23 approaches an equilibrium state at $3 \times 10^5 \text{ MC}$ steps, around which the aggregation and

1 fragmentation are closely matched in rate and the characteristic size keeps fluctuating. In order to
2 eliminate the error from the fluctuation, the equilibrium result is calculated by averaging the
3 results of the last 2×10^5 MC steps. The fractal dimension ($nf = 2.2$) was calibrated under the
4 shear condition $G = 50 \text{ s}^{-1}$, and the results for high shear condition were treated as validation
5 cases. The predicted D_{50} when the turbulent shear $G = 50 \text{ s}^{-1}$ is $90.02 \text{ }\mu\text{m}$, which is highly
6 consistent with the experiment result $88 \text{ }\mu\text{m}$. When it comes to higher turbulent shear condition,
7 the simulated median size is $56.7 \text{ }\mu\text{m}$ and appears to be slightly underestimated compared with
8 the experimental result of $69 \text{ }\mu\text{m}$. The bias for the low shear condition ($G = 50 \text{ s}^{-1}$) was mainly
9 statistical noise caused by sampling, which is inherent to any QMC approach. This error can be
10 reduced with sufficient simulation particles (Hao et al., 2013). For the high shear condition ($G =$
11 95 s^{-1}) the error of median size was 17.8 %. This error seems reasonable as a model system error,
12 as higher values (up to 27.2%) have been reported by Mietta et al. (2008). A possible reason
13 accounted for this underestimation is that the fragmentation frequency assumption or/and the
14 aggregation efficiency assumption or/and the fractal dimension are insufficient in a high-
15 intensity turbulent field. It is also critical to note that fixing the fractal dimension cannot account
16 for this error. The change of fractal dimension from the constant 2.2 to a variable term (with δ
17 calibrated using Eq. 6) would not help improving the accuracy in this case. With the calibrated
18 value $\delta = -0.046$, the error of the median size under $G = 95 \text{ s}^{-1}$ went up to 21.1%. In addition, one
19 can directly obtain the predicted FSD by the MC model at any time step. The predicted FSD at
20 MC Step = 1×10^5 , 2×10^5 , 3×10^5 , and the equilibrium state are given in Fig. 6.

21

22 Case V: Maggi's settling column experiment

1 Maggi et al. (2002, 2007) carried out a numerical study to explore the effect of variable
2 fractal dimension on the FSD in a laboratory settling column with suspended kaolinite. The
3 settling column is about 480 cm high with an inside diameter of 30 cm, above which a buffer
4 tank is set to continuously mix and dilute the highly-concentrated suspension to the test
5 concentration. The homogeneous turbulence field is produced by an oscillating 3-D grid to
6 induce flocculation. Flocs settle through the turbulent field and are recorded by the camera
7 system in the measuring section under the settling column. The experiment is performed with
8 four turbulent shear rates $G = 5, 10, 20, \text{ and } 40 \text{ s}^{-1}$ respectively and a constant sediment
9 concentration of $c = 500 \text{ mg/L}$. The density of the selected kaolinite is $\rho_s \approx 2650 \text{ kg/m}^3$ and its
10 mineral size is in the range $0.1 - 5 \text{ }\mu\text{m}$. The observation window is 6-by-6 mm^2 and the
11 resolution is $6.42 \text{ }\mu\text{m/pixel}$, which limits the scope of measurement, and overestimates the
12 number concentration.

13 The experimental FSDs for $G = 10$ and 40 s^{-1} are used to calibrate the fitting parameters
14 such as fractal dimension and fragmentation function. The other two shear rates are used to
15 validate the model results. The fitting parameters are given in Table. 1. The initial particle
16 distribution obeys a Gaussian distribution like case IV except that the D_p in this case is $2 \text{ }\mu\text{m}$. The
17 maximum floc size is selected as the Kolmogorov scale, and the fractal dimension is set variable
18 with the coefficient $\delta = -0.1$ recommended in Maggi et al. (2005, 2007, 2008).

19 The predicted and experimental results of the FSD at equilibrium state are given in Fig. 7.
20 Note that the size classes under $6.4 \text{ }\mu\text{m}$ are shown either in the FSDs in the blue shadow areas
21 with solid edges to demonstrate the level of detail this study can provide. The FSDs given by the
22 other solid lines are calculated by normalization of particle arrays excluding the particle smaller
23 than $6.4 \text{ }\mu\text{m}$, and the size classes are the same as those in Maggi et al. (2007). As can be seen in

1 Fig. 7, the predicted FSDs of the four turbulent shear rates match quite well with the
2 experimental results.

3 One can see that for the case of the lower turbulent shear rate $G = 5 \text{ s}^{-1}$, the simulated FSD
4 seems to slightly overestimate the fraction of large particles. It might be a consequence of the
5 underestimation of A_{max} in Eq. 10 for low shear rates. The term of turbulent shear is smaller when
6 the shear rate is lower, so the differential settling term is more dominant in the calculation of
7 aggregation kernel and the A_{max} would be underestimated under the simplification that
8 differential settling is zero. This leads to an overestimation of the aggregation rate of small
9 particles. Another possible reason is that the assumption of aggregation efficiency or/and
10 breakup function or/and binary fragmentation are less appropriate for kaolinite flocculation.
11 Further study and improvement will be needed to accord for it.

12 The predicted and experimental median size (D_{50}) is shown in Fig. 8. Note that the median
13 size of the experimental result is calculated by FSDs using linear interpolation. The predicted
14 and experimental results match in good accuracy. The predicted median size is getting smaller as
15 compared to the predicted result with increasing turbulent shear rate. Several reasons may be
16 accounted for this trend. Firstly, particles smaller than $6.4 \mu\text{m}$ are neglected in the experimental
17 results due to the resolution of the camera system, which would introduce a bias towards larger
18 sizes in measurement. Secondly, the selection of D_{max} or/and the assumptions about aggregation
19 efficiency and fragmentation are insufficient to represent kaolinite flocculation.

20

21 4. Discussion

22 4.1 Monte Carlo and Quasi-Monte Carlo sampling

1 In this section, a numerical example, combining aggregation and fragmentation where an
 2 exact analytical solution is known (case V in section 3), is used to compare the accuracy and
 3 efficiency of different QMC methods and the LHS scheme described above with the standard
 4 MC scheme. MC simulations run in a PC equipped with a CPU of Intel(R) Core(TM) i7-9750H
 5 CPU @2.60GHz and memory of 16 GB. The error that describes how well the FSD
 6 approximates the analytical solution is defined as

$$7 \quad E_r = \sum_{i=1}^{N_c} |n_i(D, t) - n_i^A(D, t)| \quad (30)$$

8 where $N_c = 10$ is the number of size classes, the superscript A indicates the analytical solution.
 9 The simulations were conducted with different numbers of particles $N = 15,000, 30,000, 75,000,$
 10 and $150,000$, and the MC steps were set to $5 \times 10^5, 5 \times 10^5, 7 \times 10^5,$ and 15×10^5 respectively to
 11 make sure that equilibrium is reached.

12 The FSDs results of all the schemes converge towards the analytical solution as N increases
 13 (Fig. 9). Note that the errors of all schemes decrease significantly when N is larger than $30,000$,
 14 and the benefit (reduction of error) decreases with further increase of N . In addition, errors of
 15 two QMC methods and the LHS scheme are always smaller than standard MC methods using
 16 pseudorandom numbers (also see Table 1). The result simulated using the Halton sequence
 17 reaches the highest accuracy when N is larger than $30,000$. In other words, compared to the other
 18 three schemes, the QMC scheme using Halton sequence requires the least particle numbers in
 19 simulated system to reach reasonable accuracy ($E_r < 0.055$ in this case).

20 The computational costs of the four different MC methods are also tested (Fig. 10). Since
 21 the producing algorithm of quasi-numbers induces extra cost or/and the codes might not be
 22 optimized yet, the time consumptions of pre-producing random number series are not included.
 23 In addition, the time consumption of simulation with LHS sequence is not tested due to its low

1 efficiency of pre-production. The required CPU time of QMC schemes using Sobol' and Halton
 2 sequences with any number of particles N are less than the standard MC method (Fig. 10 and
 3 Table 2). The simulation using Halton sequence saved more CPU time compared to that by using
 4 other two random number series when N is larger than 30,000. Note that the CPU time reduction
 5 of QMC compared to standard MC is around 8% with particle numbers $N = 1.5 \times 10^5$. It is
 6 reasonable to expect that the QMC method would save more calculation cost in solving the high
 7 dimensional problem (e.g. bio-adhesion included PBM).

8

9 4.2 Sensitivity tests

10 (1) Breakage events

11 The fragmentation distribution function plays an important role in predicting the steady-
 12 state FSD and characteristic sizes (Maggi, 2005; Khelifa and Hill, 2006; Shin et al., 2015).
 13 However, there were only simple theoretical assumptions about the fragmentation distribution
 14 since it is still difficult to carry out laboratory experiment to observe the micro-scale
 15 fragmentation processes directly (Maggi, 2005; Spicer and Pratsinis, 1996). In order to explore
 16 the influence of different fragmentation distribution functions on the modeling results, the three
 17 simplest assumptions, including binary breakup with mass ratio 1:1 (Eq. 12), ternary breakup
 18 with mass ratio 1:1:2 (Eq. 31), and uniform breakup (Eq. 24~25) (e.g., Spicer and Pratsinis, 1996;
 19 Shen and Maa, 2015,2016), are tested in the model and compared to the experimental data with
 20 different turbulent shear rates by Maggi et al. (2007).

$$21 \quad \begin{cases} N_{fi'} = r_4 N_{fi} \\ N_{fi''} = N_{fi'''} = (1 - r_4) N_{fi} / 2 \end{cases} \quad (31)$$

22 The results given in Fig. 11 show that different fragmentation distribution functions will
 23 lead to significantly different predictions. Compared to the binary breakup assumption, the

1 predicted FSDs from the ternary and the uniform breakup assumptions are skewed towards
2 smaller size classes. The predicted median sizes simulated by using binary breakup function are
3 higher than those by the other two assumptions. The results of the median sizes show a tendency
4 that more fragments are produced after each fragmentation event, which will result in lower
5 median sizes. This is to be expected since the mean size of fragments is smaller than that with
6 assumptions of less fragments.

7 It seems that using the binary fragmentation gives a much better match of both FSDs and
8 median sizes. This assumption seems reasonable since Kramer and Clark (1999) proposed that
9 the probability for a floc breaking into multiple fragments is small, and Tsai and Hwang (1995)
10 found that flocs are prone to binary breakup into fragments with similar size. From another
11 perspective, breakage into multiple fragments, which occurs infrequently, can be seen as several
12 simultaneous binary fragmentation events. Nevertheless, selection of the breakage distribution
13 function still requires a better understanding of floc structure (e.g., fractal property, density) and
14 the breakup process under hydrodynamic impact.

15

16 (2) Effects of fractal dimension

17 The fractal dimension nf is used to empirically relate the geometry of flocs to their density,
18 strength and settling velocity. Usually, nf is estimated from experimental floc size and settling
19 velocity data. Note that the fractal dimension of flocs with even the same size may be different
20 since flocs might not be self-similar at all, which is the basic assumption in the definition of
21 fractal dimension. Most studies usually assume a constant nf on empirical understanding
22 (Winterwerp, 1998), or an exponent form nf based on the knowledge that large particles have
23 low nf than smaller particles (Khelifa and Hill, 2006; Maggi et al., 2007). Son and Hsu (2008)

1 found that a change of fractal dimension (from a constant to a power law) does not obviously
 2 improve the estimation of steady-state median size. Khelifa and Hill (2006) proposed an
 3 estimation of the coefficient δ in Eq. 1:

$$4 \quad \delta = \frac{\log(F_c/3)}{\log(D_{fc}/D_p)} \quad (32)$$

5 where $D_{fc} = 2,000 \mu\text{m}$ and $F_c = 2$ are suggested in Khelifa and Hill (2006).

6 As is shown in Fig. 12, the predicted FSDs at steady state are quite sensitive to the fractal
 7 dimension nf . Using the constant $nf = 2.2$, both the modelling FSD skews toward the larger
 8 classes and the median size is larger than that by using the constant $nf = 2.0$. This is expected
 9 since flocs with a higher fractal dimension are more solid than those with a low fractal dimension.
 10 Another reason may be that the differential settling term in Eq. 2 becomes more important
 11 relative to the turbulent shear term since the velocity differences between small flocs and big
 12 flocs are significant compared to the case of low nf . Results from using a variable nf show a
 13 higher accuracy with experimental data. The value of coefficient $\delta = -0.1$ suggested by Maggi et
 14 al. (2005, 2007, 2008) matched quite well both the FSDs and the median sizes.

15 However, it is worth to mention that the predicted median sizes using constant nf and
 16 variable nf by Eq. 32 decrease rapidly with the turbulent shear increasing. In other words, the
 17 relative errors of D_{50} of those three cases using different nf reduced to nearly 30% when the
 18 turbulent shear rate is high. It might indicate that the calculation of differential settling (Eq. 4) is
 19 overestimated when the turbulent shear rate is low. In addition, the maximum aggregation kernel
 20 A_{\max} calculated by Eq. 5 neglects the effect of differential settling, which may cause an error
 21 when the turbulent shear rate is low to some extent.

1 It is widely accepted that the density of the flocs decrease as a function of floc size. To
 2 better investigate their relationship, the variations of the excess density of the flocs were also
 3 simulated.

$$4 \quad \Delta\rho_f \propto (\rho_s - \rho_w) \left[\frac{D_p}{D_f} \right]^{3-n_f} \quad (33)$$

5 where $\rho_w = 1000 \text{ kg/m}^3$ is the density of water. Under the turbulent shear rate $G = 40 \text{ s}^{-1}$, it can be
 6 seen that the floc size increases while the floc density decreases with QMC steps, which indicates
 7 that the density of the flocs often decrease as a function of floc size (Fig. 13).

8

9 4.3 Connections with field-scale sediment models

10 With the rapid growth of computational ability, a large quantity of field-scale numerical
 11 models for simulating hydrodynamics and sediment transport have been developed in recent
 12 decades. According to the consideration of computational spatial dimension, these numerical
 13 models can be classified as one-dimensional models (e.g., MOBED and FLUVIAL 11), 2-
 14 dimensional models (e.g., SERATRA, Delft 2D and MIKE 21), and 3-dimensional models (e.g.,
 15 TELEMAC, Delft 3D, and ROMS) (Krishnappan, 1981; Chang, 1984; Onishi and Wise, 1982;
 16 Walstra et al., 1998; Warren and Bach, 1992; Hervouet and Bates, 2000; Delft Hydraulic, 1999;
 17 Song and Haidvogel, 1994). One of the most important parameters in simulating sediment
 18 transport and estuarine and coastal evolution is the settling velocity (w_s) of cohesive sediments,
 19 which is controlled by floc size, floc shape, and floc density. However, the settling velocity is
 20 often treated as an arbitrary (although reasonable) constant or a fitting parameter in most field-
 21 scale models. However, it usually does not match the measured w_s (Papanicolaou et al, 2008;
 22 Toorman, 2012; Horemans et al., 2020). The lack of understanding of flocculation mechanisms
 23 would cause biased estimations in large-scale simulation for sediment transport processes.

1 Numerical models focused on multi-class cohesive sediment flocculation often give a better
2 estimation of the settling flux but consume more computing resources with an increasing number
3 of size classes (Lee et al, 2011; Toorman, 2012; Zhang et al., 2013; Shen and Maa, 2017). The
4 PBM framework contains external and internal variables: the former describe the physical space
5 of the location of particles, and the latter account for one or several distinguishable properties of
6 particles such as size, volume, and biomass fraction (Shen and Maa, 2016; Iveson, 2002). The
7 computational resources of PBM increase rapidly with the inclusion of additional internal
8 variables. Thus, the PBM accounting for size in any 3-D model (i.e., with three external variables
9 x , y , and z) is actually a 4-D model, which demands expensive computational costs and thus has
10 not been widely adopted consequently. Nevertheless, simplified PBMs, e.g., the two-class PBM
11 (Lee et al., 2011) and the three-class PBM (Shen et al., 2018a, 2018b), have already been
12 employed in cohesive sediment studies. There is still a broad space for multiple class PBMs to be
13 investigated in cohesive sediment field.

14 It is also crucial to note that methods such as the simplified Lagrangian model (Winterwerp,
15 1998) and the PBM solved by the discretization method (e.g., Krishnappan and Marsalek, 2002;
16 Liu et al., 2019; Verney et al., 2011) or the quadrature method of moments (e.g., Shen and Maa,
17 2015, 2016; Li et al., 2019) have explicit mathematical formulae. They are in favor of being
18 coupled into hydrodynamic models to simulate cohesive sediment transport process. For instance,
19 Krishnappan and Marsalek (2002) proposed a coupled 1-D advection-diffusion and pure-
20 aggregation PBM to predict the sediment flocs from an on-stream stormwater management pond,
21 and Liu et al. (2019) implemented the PBM in a large eddy simulation of wave-driven Langmuir
22 turbulence. On the other hand, the QMC models cannot be directly coupled with field-scale
23 model in estuarine and coastal waters at current stage. Regarding the application of stochastic

1 methods in modeling the flocculation process, most of the existing works are based on the
2 Winterwerp's formula. For example, Maggi (2008) proposed a stochastic Lagrangian model to
3 explore the temporal variability of the median floc size, similar as shown in Fig.6(a)(b), and Shin
4 et al. (2015) adopted a MC method to determine the breakup probability and could calculate the
5 FSD in log-normal forms. Nevertheless, their models seem difficult to extend to account for
6 flocculation of bio-mineral aggregates with multi-modal FSDs due to the uncertainty and
7 complexity of biomass-sediment interaction (Shen et al., 2019).

8 The QMC models produce a new stochastic way to solve PBM and help determining
9 various micro-scale flocculation behaviors, which provides new prospects to improve low cost
10 bio-flocculation models to couple with large-scale model. Possibly coupled with computational
11 fluid dynamics (CFD) in turbulent flow (Liu and Chan, 2017; Xu et al., 2017), the QMC based
12 PBMs also have the potential to simulate the interactions between turbulence and flocculated
13 particles in the future.

14

15 5. Conclusions

16 The following conclusions can be drawn for this study:

- 17 (1) The quasi-Monte Carlo method is applied to develop a flocculation model by a size-
18 based population balance model for cohesive sediments. The maximum relative errors
19 of the mean sizes are less than 10%.
- 20 (2) The settling column experimental results for suspended kaolinite with a concentration of
21 500 mg/L and different shear rates carried out by Maggi et al. (2002) are used to
22 validate the simulated FSD and its median size. The QMC model predicted these well
23 by selecting similar coefficients in aggregation and fragmentation processes given by

1 Mietta et al. (2008). The results of simulated median size for a laboratory experiment
2 conducted by Tran and Strom (2017) also show a reasonable agreement.

3 (3) The calculation accuracies and time consumptions of different QMC schemes and the
4 LHS scheme were tested. All three considered low-discrepancy number schemes show
5 better accuracy than the standard MC method, among which the QMC scheme using the
6 Halton sequence is the best one in accuracy. On the other side, compared to the other
7 schemes, the QMC scheme with Halton sequence requires the least particle numbers in
8 simulated system to reach a reasonable accuracy. The CPU time of schemes using the
9 Halton sequence and the Sobol' sequence are less than that of standard MC. In this case,
10 one can save around 8% CPU time with $N = 1.5 \times 10^5$ by replacing the pseudorandom
11 number by the Halton sequence.

12 (4) The model prediction will be significantly influenced by assumptions on the fractal
13 dimension nf and fragmentation distribution functions, which should be checked
14 carefully in every model for different applications.

15 (5) The reasonable performance of the QMC model for cohesive sediments shows great
16 prospect in solving multivariate and high dimensional problem (e.g. biomass effect on
17 flocculation) due to its nature of discretion.

1 Acknowledgments

2 The authors would like to acknowledge the funding support from the National Natural
3 Science Foundation of China (Grant No. U2040203 & 51909068 & 52011540388), the
4 Fundamental Research Funds for the Central Universities of China (Grant No. B200201009), the
5 Research Funds of Shanghai Municipal Water Authority (Grant No. 2020-02), the Open Funds
6 of the Key Laboratory of Ministry of Education for Coastal Disaster and Protection of China
7 (Grant No. 201901 & 202004), and the Open Funds of State Key Laboratory of Hydraulic
8 Engineering Simulation and Safety of China (Grant No. HESS-1917). This study was also
9 supported under the framework of international cooperation program managed by the National
10 Research Foundation of Korea (2020K2A9A2A06036472, FY2020).

12 References

- 13 Azhikodan, G., Yokoyama, K., 2021. Erosion and sedimentation pattern of fine sediments and its
14 physical characteristics in a macrotidal estuary. *Science of The Total Environment* 753,
15 142025. <https://doi.org/10.1016/j.scitotenv.2020.142025>
- 16 Bertin, D., Cotabarren, I., Piña, J., Bucalá, V., 2016. Population balance discretization for
17 growth, attrition, aggregation, breakage and nucleation. *Computers & Chemical*
18 *Engineering* 84, 132-150. <https://doi.org/10.1016/j.compchemeng.2015.08.011>
- 19 Burchard, H., Schuttelaars, H.M., Ralston, D.K., 2018. Sediment Trapping in Estuaries. *Annual*
20 *Review of Marine Science* 10, 371-395. [https://doi.org/10.1146/annurev-marine-010816-](https://doi.org/10.1146/annurev-marine-010816-060535)
21 [060535](https://doi.org/10.1146/annurev-marine-010816-060535)
- 22 Burhenne, S., Jacob, D., Henze, G.P., 2011. Sampling based on Sobol' sequences for Monte
23 Carlo techniques applied to building simulations. In: *Proceedings of Building Simulation*

- 1 2011: 12th Conference of International Building Performance Simulation Association.
2 Sydney, Australia, 14-16 November 2011, pp. 1816-1823.
- 3 Caflich, R.E., 1998. Monte carlo and quasi-monte carlo methods. *Acta Numerica* 7, 1-49.
4 <https://doi.org/10.1017/S0962492900002804>
- 5 Chang, H. H, 1984. Modeling of river channel changes. *Journal of Hydraulic Engineering*
6 110(2), 157-172. [https://doi.org/10.1061/\(ASCE\)0733-9429\(1984\)110:2\(157\)](https://doi.org/10.1061/(ASCE)0733-9429(1984)110:2(157))
- 7 Chi, H., Mascagni, M., Warnock, T., 2005. On the optimal Halton sequence. *Mathematics and*
8 *Computers in Simulation* 70(1), 9-21. <https://doi.org/10.1016/j.matcom.2005.03.004>
- 9 Das, A., Bück, A., Kumar, J., 2020. Selection function in breakage processes: PBM and Monte
10 Carlo modeling. *Advanced Powder Technology* 31(4), 1457-1469.
11 <https://doi.org/10.1016/j.appt.2020.01.002>
- 12 Dick, J., Kuo, F.Y., Sloan, I.H., 2013. High-dimensional integration: The quasi-Monte Carlo way.
13 *Acta Numerica* 22, 133-288. <https://doi.org/10.1017/S0962492913000044>
- 14 Edmonds, D.A., Slingerland, R.L., 2010. Significant effect of sediment cohesion on delta
15 morphology. *Nature Geoscience* 3(2), 105-109. <https://doi.org/10.1038/ngeo730>
- 16 Eibeck, A., Wagner, W., 2001. Stochastic particle approximations for Smoluchoski's coagulation
17 equation. *Annals of Applied Probability* 11, 1137-1165. <https://doi.org/10.2307/2699912>
- 18 Fall, K. A., Friedrichs, C. T., Massey, G. M., Bowers, D. G., Smith, S. J., 2021. The importance
19 of organic content to fractal floc properties in estuarine surface waters: Insights from video,
20 LISST, and pump sampling. *Journal of Geophysical Research: Oceans*, 2020JC016787.
21 <https://doi.org/10.1029/2020JC016787>

- 1 Garcia, A.L., Van Den Broeck, C., Aertsens, M., Serneels, R., 1987. A Monte Carlo simulation
2 of coagulation. *Physica A: Statistical Mechanics and its Applications* 143(3), 535-546.
3 [https://doi.org/10.1016/0378-4371\(87\)90164-6](https://doi.org/10.1016/0378-4371(87)90164-6)
- 4 Geyer, W.R., MacCready, P., 2014. The Estuarine Circulation. *Annual Review of Fluid*
5 *Mechanics* 46, 175-197. <https://doi.org/10.1146/annurev-fluid-010313-141302>
- 6 Halton, J.H., 1960. On the efficiency of certain quasi-random sequences of points in evaluating
7 multi-dimensional integrals. *Numerische Mathematik* 2(1), 84-90.
- 8 Hao, X., Zhao, H., Xu, Z., Zheng, C., 2013. Population balance-Monte Carlo simulation for gas-
9 to-particle synthesis of nanoparticles. *Aerosol science and technology*, 47(10), 1125-1133.
10 <https://doi.org/10.1080/02786826.2013.823642>
- 11 Hervouet, J. M., Bates, P., 2000. The TELEMAC modelling system. *Hydrological Processes*
12 14(13).
- 13 Hess, S., Polak, J., 2003. An alternative method to the scrambled Halton sequence for removing
14 correlation between standard Halton sequences in high dimensions. In: *43rd Congress of the*
15 *European Regional Science Association: "Peripheries, Centres, and Spatial Development in*
16 *the New Europe"*, Jyväskylä, Finland, August 2003. <http://hdl.handle.net/10419/116163>
- 17 Horemans, D. M. L., Dijkstra, Y. M., Schuttelaars, H. M., Meire, P., Cox, T. J. S., 2020.
18 Unraveling the Essential Effects of Flocculation on Large-Scale Sediment Transport
19 Patterns in a Tide-Dominated Estuary. *Journal of Physical Oceanography* 50(7), 1957-1981.
20 <https://doi.org/10.1175/JPO-D-19-0232.1>
- 21 Hou, T., Nuyens, D., Roels, S., Janssen, H., 2019. Quasi-Monte Carlo based uncertainty analysis:
22 Sampling efficiency and error estimation in engineering applications. *Reliability*
23 *Engineering & System Safety* 191, 106549. <https://doi.org/10.1016/j.res.2019.106549>

- 1 Hydraulics, D., 1999. Delft3D users' manual. *Delft Hydraulics, The Netherlands*.
- 2 Iveson, S. M., 2002. Limitations of one-dimensional population balance models of wet
3 granulation processes. *Powder Technology*, 124(3), 219-229. [https://doi.org/10.1016/S0032-](https://doi.org/10.1016/S0032-5910(02)00026-8)
4 [5910\(02\)00026-8](https://doi.org/10.1016/S0032-5910(02)00026-8)
- 5 Kariwala, V., Cao, Y., K. Nagy, Z., 2012. Automatic differentiation-based quadrature method of
6 moments for solving population balance equations. *AIChE Journal* 58(3), 842-854.
7 <https://doi.org/10.1002/aic.12613>
- 8 Keramat, M., Kielbasa, R., 1997. Latin hypercube sampling Monte Carlo estimation of average
9 quality index for integrated circuits. *Analog Integrated Circuits and Signal Processing*
10 14(1-2), 131-142.
- 11 Keyvani, A., Strom, K., 2014. Influence of cycles of high and low turbulent shear on the growth
12 rate and equilibrium size of mud flocs. *Marine Geology* 354, 1-14.
13 <https://doi.org/10.1016/j.margeo.2014.04.010>
- 14 Khelifa, A., Hill, P., 2006. Kinematic assessment of floc formation using a Monte Carlo model.
15 *Journal of Hydraulic Research* 44(4), 548-559.
16 <https://doi.org/10.1080/00221686.2006.9521705>
- 17 Khelifa, A., Hill, P.S., Lee, K., 2005. Assessment of minimum sediment concentration for OMA
18 formation using a Monte Carlo model, in: Al-Azab, M., El-Shorbagy, W. (Eds.),
19 *Developments in Earth and Environmental Sciences*. Elsevier, pp. 93-104.
20 [https://doi.org/10.1016/S1571-9197\(05\)80031-X](https://doi.org/10.1016/S1571-9197(05)80031-X)
- 21 Kiørboe, T., Andersen, K. P., Dam, H. G., 1990. Coagulation efficiency and aggregate formation
22 in marine phytoplankton. *Marine Biology*, 107(2), 235-245.
23 <https://doi.org/10.1007/BF01319822>

- 1 Kotalczyk, G., Kruis, F.E., 2017. A Monte Carlo method for the simulation of coagulation and
2 nucleation based on weighted particles and the concepts of stochastic resolution and
3 merging. *Journal of Computational Physics* 340, 276-296.
4 <https://doi.org/10.1016/j.jcp.2017.03.041>
- 5 [Kramer, T. A., Clark, M. M., 1999. Incorporation of aggregate breakup in the simulation of](#)
6 [orthokinetic coagulation. *Journal of colloid and interface science*, 216\(1\), 116-126.](#)
7 <https://doi.org/10.1006/jcis.1999.6305>
- 8 Krishnappan, B. G, 1981. User's manual: Unsteady, non-uniform, mobile boundary flow
9 model—MOBED. *Hydraulic Division, National Water Research Institute, CCIW,*
10 *Burlington, Ontario*
- 11 Krishnappan, B. G., Marsalek, J., 2002. Modelling of flocculation and transport of cohesive
12 sediment from an on-stream stormwater detention pond. *Water Research*, 36(15), 3849-
13 3859. [https://doi.org/10.1016/S0043-1354\(02\)00087-8](https://doi.org/10.1016/S0043-1354(02)00087-8)
- 14 Kruis, F.E., Maisels, A., Fissan, H., 2000. Direct simulation Monte Carlo method for particle
15 coagulation and aggregation. *AIChE Journal* 46(9), 1735-1742.
16 <https://doi.org/10.1002/aic.690460905>
- 17 Kumar, S., Ramkrishna, D., 1996. On the solution of population balance equations by
18 discretization—I. A fixed pivot technique. *Chemical Engineering Science* 51(8), 1311-1332.
19 [https://doi.org/10.1016/0009-2509\(96\)88489-2](https://doi.org/10.1016/0009-2509(96)88489-2)
- 20 Kumar, J., Kaur, G., Tsotsas, E., 2016. An accurate and efficient discrete formulation of
21 aggregation population balance equation. *Kinetic & Related Models* 9(2), 373.
22 <https://doi.org/10.3934/krm.2016.9.373>
- 23 Kuprenas, R., Tran, D., Strom, K., 2018. A shear-limited flocculation model for dynamically

- 1 predicting average floc size. *Journal of Geophysical Research: Oceans*, 123(9), 6736-6752.
2 <https://doi.org/10.1029/2018JC014154>
- 3 Lai, H., Fang, H., Huang, L., He, G., Reible, D., 2018. A review on sediment bioflocculation:
4 Dynamics, influencing factors and modeling. *Science of the total environment*, 642, 1184-
5 1200. <https://doi.org/10.1016/j.scitotenv.2018.06.101>
- 6 Lee, B.J., Toorman, E., Molz, F.J., Wang, J., 2011. A two-class population balance equation
7 yielding bimodal flocculation of marine or estuarine sediments. *Water Research* 45(5),
8 2131-2145. <https://doi.org/10.1016/j.watres.2010.12.028>
- 9 Lee, B. J., Molz, F., 2014. Numerical simulation of turbulence-induced flocculation and
10 sedimentation in a flocculant-aided sediment retention pond. *Environmental Engineering*
11 *Research*, 19(2), 165-174. <https://doi.org/10.4491/eer.2014.19.2.165>
- 12 Lee, K.F., Patterson, R.I.A., Wagner, W., Kraft, M., 2015. Stochastic weighted particle methods
13 for population balance equations with coagulation, fragmentation and spatial
14 inhomogeneity. *Journal of Computational Physics* 303, 1-18.
15 <https://doi.org/10.1016/j.jcp.2015.09.031>
- 16 Li, D., Li, Z., Gao, Z., 2019. Quadrature-based moment methods for the population balance
17 equation: An algorithm review. *Chinese Journal of Chemical Engineering* 27(3), 483-500.
18 <https://doi.org/10.1016/j.cjche.2018.11.028>
- 19 Liffman, K., 1992. A Direct Simulation Monte Carlo Method for Cluster Coagulation. *Journal of*
20 *Computational Physics* 100(1), 116-127. [https://doi.org/10.1016/0021-9991\(92\)90314-O](https://doi.org/10.1016/0021-9991(92)90314-O)
- 21 Lin, Y., Lee, K., Matsoukas, T., 2002. Solution of the population balance equation using
22 constant-number Monte Carlo. *Chemical Engineering Science* 57(12), 2241-2252.
23 [https://doi.org/10.1016/S0009-2509\(02\)00114-8](https://doi.org/10.1016/S0009-2509(02)00114-8)

- 1 Liu, J., Liang, J. H., Xu, K., Chen, Q., Ozdemir, C. E., 2019. Modeling sediment flocculation in
2 Langmuir turbulence. *Journal of Geophysical Research: Oceans*, 124(11), 7883-7907.
3 <https://doi.org/10.1029/2019JC015197>
- 4 Liu, S., Chan, T. L., 2017. A coupled CFD-Monte Carlo method for simulating complex aerosol
5 dynamics in turbulent flows. *Aerosol Science and Technology*, 51(3), 269-281.
6 <https://doi.org/10.1080/02786826.2016.1260087>
- 7 Maggi, F., 2005. Flocculation dynamics of cohesive sediment. (Ph.D. Dissertation) *Delft*
8 *University of Technology*, Netherlands.
- 9 Maggi, F., 2008. Stochastic flocculation of cohesive sediment: analysis of floc mobility within
10 the floc size spectrum. *Water Resources Research* 44(1).
11 <https://doi.org/10.1029/2007WR006109>
- 12 Maggi, F., Mietta, F., Winterwerp, J.C., 2007. Effect of variable fractal dimension on the floc
13 size distribution of suspended cohesive sediment. *Journal of Hydrology* 343(1-2), 43-55.
14 <https://doi.org/10.1016/j.jhydrol.2007.05.035>
- 15 Maggi, F., Winterwerp, J., Fontijn, H., van Kesteren, W., Cornelisse, J., 2002. A settling column
16 for turbulence-induced flocculation of cohesive sediments, in: Tony L. Wahl, Clifford A.
17 Pugh, Kevin A. Oberg, and Tracy B. Vermeyen (Eds.), *Hydraulic Measurements and*
18 *Experimental Methods 2002*, pp. 1-10.
- 19 Marchisio, D.L., Pikturna, J.T., Fox, R.O., Vigil, R.D., Barresi, A.A., 2003a. Quadrature method
20 of moments for population-balance equations. *AIChE Journal* 49(5), 1266–1276.
21 <https://doi.org/10.1002/aic.690490517>

- 1 Marchisio, D.L., Vigil, R.D., Fox, R.O., 2003b. Quadrature method of moments for aggregation–
2 breakage processes. *Journal of Colloid and Interface Science* 258(2), 322-334.
3 [https://doi.org/10.1016/S0021-9797\(02\)00054-1](https://doi.org/10.1016/S0021-9797(02)00054-1)
- 4 Mascagni, M., Chi, H., 2004. On the scrambled halton sequence. *Monte Carlo Methods and*
5 *Applications* 10(3-4), 435-442. <https://doi.org/10.1515/mcma.2004.10.3-4.435>
- 6 McCave, I., 1984. Size spectra and aggregation of suspended particles in the deep ocean. Deep
7 Sea Research Part A. *Deep Sea Research Part A. Oceanographic Research Papers* 31(4),
8 329-352. [https://doi.org/10.1016/0198-0149\(84\)90088-8](https://doi.org/10.1016/0198-0149(84)90088-8)
- 9 McCoy, B.J., Madras, G., 2003. Analytical solution for a population balance equation with
10 aggregation and fragmentation. *Chemical Engineering Science* 58(13), 3049-3051.
11 [https://doi.org/10.1016/S0009-2509\(03\)00159-3](https://doi.org/10.1016/S0009-2509(03)00159-3)
- 12 McGraw, R., 1997. Description of aerosol dynamics by the quadrature method of moments.
13 *Aerosol Science and Technology* 27(2), 255-265.
14 <https://doi.org/10.1080/02786829708965471>
- 15 McKay, M., Beckman, R., 1979. A comparison of three methods for selecting values of input
16 variables in the analysis of output from a computer code. *Technometrics* 21(2).
17 <https://doi.org/10.1080/00401706.1979.10489755>
- 18 Mietta, F., Maggi, F., Winterwerp, J.C., 2008. Chapter 19 Sensitivity to breakup functions of a
19 population balance equation for cohesive sediments. INTERCOH 2005. *Sediment and*
20 *Ecohydraulics* 9, pp. 275-286. [https://doi.org/10.1016/S1568-2692\(08\)80021-6](https://doi.org/10.1016/S1568-2692(08)80021-6)
- 21 Mietta, F., Chassagne, C., Verney, R., Winterwerp, J. C., 2011. On the behavior of mud floc size
22 distribution: model calibration and model behavior. *Ocean Dynamics*, 61(2-3), 257-271.
23 <https://doi.org/10.1007/s10236-010-0330-2>

- 1 Olsson, A., Sandberg, G., Dahlblom, O., 2003. On Latin hypercube sampling for structural
2 reliability analysis. *Structural safety* 25(1), 47-68. [https://doi.org/10.1016-](https://doi.org/10.1016/S0167-4730(02)00039-5)
3 [4730\(02\)00039-5](https://doi.org/10.1016/S0167-4730(02)00039-5)
- 4 Olsson, A.M., Sandberg, G.E., 2002. Latin hypercube sampling for stochastic finite element
5 analysis. *Journal of Engineering Mechanics* 128(1), 121-125.
6 [https://doi.org/10.1061/\(ASCE\)0733-9399\(2002\)128:1\(121\)](https://doi.org/10.1061/(ASCE)0733-9399(2002)128:1(121))
- 7 Onishi, Y., Wise, S. E., 1982. SERATRA: User's manual for the instream sediment-contaminant
8 transport model. *Technical Rep. No. PB-83e122739 (Pacific Northwest Laboratory,*
9 *Battelle-Northwest, Richland, Wash).*
- 10 Papanicolaou, A. T. N., Elhakeem, M., Krallis, G., Prakash, S., Edinger, J., 2008. Sediment
11 transport modeling review—current and future developments. *Journal of hydraulic*
12 *engineering* 134(1), 1-14. [https://doi.org/10.1061/\(ASCE\)0733-9429\(2008\)134:1\(1\)](https://doi.org/10.1061/(ASCE)0733-9429(2008)134:1(1))
- 13 Passalacqua, A., Laurent, F., Madadi-Kandjani, E., Heylmun, J.C., Fox, R.O., 2018. An open-
14 source quadrature-based population balance solver for OpenFOAM. *Chemical Engineering*
15 *Science* 176, 306-318. <https://doi.org/10.1016/j.ces.2017.10.043>
- 16 Radović, I., Sobol, I.M., Tichy, R.F., 1996. Quasi-Monte Carlo methods for numerical
17 integration: Comparison of different low discrepancy sequences. *Monte Carlo Methods and*
18 *Applications* 2(1), 1-14. <https://doi.org/10.1515/mcma.1996.2.1.1>
- 19 Scott, W.T., 1968. Analytic studies of cloud droplet coalescence I. *Journal of the atmospheric*
20 *sciences* 25(1), 54-65. [https://doi.org/10.1175/1520-](https://doi.org/10.1175/1520-0469(1968)025<0054:ASOCDC>2.0.CO;2)
21 [0469\(1968\)025<0054:ASOCDC>2.0.CO;2](https://doi.org/10.1175/1520-0469(1968)025<0054:ASOCDC>2.0.CO;2)

- 1 Shen, X., Maa, J.P.Y., 2015. Modeling floc size distribution of suspended cohesive sediments
2 using quadrature method of moments. *Marine Geology* 359, 106-119.
3 <https://doi.org/10.1016/j.margeo.2014.11.014>
- 4 Shen, X., Maa, J.P.Y., 2016. Numerical simulations of particle size distributions: Comparison
5 with analytical solutions and kaolinite flocculation experiments. *Marine Geology* 379, 84-
6 99. <https://doi.org/10.1016/j.margeo.2016.05.014>
- 7 Shen, X., Maa, J.P.-Y., 2017. Floc size distributions of suspended kaolinite in an advection
8 transport dominated tank: measurements and modeling. *Ocean Dynamics* 67, 1495-1510.
9 <https://doi.org/10.1007/s10236-017-1097-5>
- 10 Shen, X., Lee, B. J., Fettweis, M., Toorman, E. A., 2018a. A tri-modal flocculation model
11 coupled with TELEMAC for estuarine muds both in the laboratory and in the field. *Water*
12 *research*, 145, 473-486. <https://doi.org/10.1016/j.watres.2018.08.062>
- 13 Shen, X., Toorman, E.A., Lee, B.J., Fettweis, M., 2018b. Biophysical flocculation of suspended
14 particulate matters in Belgian coastal zones. *Journal of Hydrology* 567, 238-252.
15 <https://doi.org/10.1016/j.jhydrol.2018.10.028>
- 16 Shen, X., Toorman, E. A., Lee, B. J., Fettweis, M., 2019. An approach to modeling biofilm
17 growth during the flocculation of suspended cohesive sediments. *Journal of Geophysical*
18 *Research: Oceans* 124(6), 4098-4116. <https://doi.org/10.1029/2018JC014493>
- 19 Shiea, M., Buffo, A., Vanni, M., Marchisio, D., 2020. Numerical Methods for the Solution of
20 Population Balance Equations Coupled with Computational Fluid Dynamics. *Annual review*
21 *of chemical and biomolecular engineering* 11, 339-366. [https://doi.org/10.1146/annurev-
22 chembioeng-092319-075814](https://doi.org/10.1146/annurev-chembioeng-092319-075814)

- 1 Shin, H.J., Son, M., Lee, G.-h., 2015. Stochastic flocculation model for cohesive sediment
2 suspended in water. *Water* 7(5), 2527-2541. <https://doi.org/10.3390/w7052527>
- 3 Singh, M., Vuik, K., Kaur, G., Bart, H.-J., 2019. Effect of different discretizations on the
4 numerical solution of 2D aggregation population balance equation. *Powder Technology* 342,
5 972-984. <https://doi.org/10.1016/j.powtec.2018.10.028>
- 6 Singhee, A., Rutenbar, R.A., 2010. Why quasi-monte carlo is better than monte carlo or latin
7 hypercube sampling for statistical circuit analysis. *IEEE Transactions on Computer-Aided*
8 *Design of Integrated Circuits and Systems* 29(11), 1763-1776.
9 <https://doi.org/10.1109/TCAD.2010.2062750>
- 10 Smith, M., Matsoukas, T., 1998. Constant-number Monte Carlo simulation of population
11 balances. *Chemical Engineering Science* 53(9), 1777-1786. [https://doi.org/10.1016/S0009-](https://doi.org/10.1016/S0009-2509(98)00045-1)
12 [2509\(98\)00045-1](https://doi.org/10.1016/S0009-2509(98)00045-1)
- 13 Smoluchowski, M., 1917. Versuch einer mathematischen Theorie der Koagulationskinetik
14 kolloider Lösungen. *Zeitschrift für Physikalische Chemie* 92, 129–168. (in German)
- 15 Sobol', I.y.M., 1967. On the distribution of points in a cube and the approximate evaluation of
16 integrals. *USSR Computational Mathematics and Mathematical Physics* 7(4), 86-112.
17 [https://doi.org/10.1016/0041-5553\(67\)90144-9](https://doi.org/10.1016/0041-5553(67)90144-9)
- 18 Sobol, I.M., 1998. On quasi-monte carlo integrations. *Mathematics and computers in simulation*
19 47(2-5), 103-112. [https://doi.org/10.1016/S0378-4754\(98\)00096-2](https://doi.org/10.1016/S0378-4754(98)00096-2)
- 20 Son, M., Hsu, T. J., 2008. Flocculation model of cohesive sediment using variable fractal
21 dimension. *Environmental Fluid Mechanics*, 8(1), 55-71. [https://doi.org/10.1007/s10652-](https://doi.org/10.1007/s10652-007-9050-7)
22 [007-9050-7](https://doi.org/10.1007/s10652-007-9050-7)

- 1 Son, M., Hsu, T. J., 2009. The effect of variable yield strength and variable fractal dimension on
2 flocculation of cohesive sediment. *Water Research*, 43(14), 3582-3592.
3 <https://doi.org/10.1016/j.watres.2009.05.016>
- 4 Song, Y., Haidvogel, D., 1994. A semi-implicit ocean circulation model using a generalized
5 topography-following coordinate system. *Journal of Computational Physics* 115(1), 228-
6 244. <https://doi.org/10.1006/jcph.1994.1189>
- 7 Spicer, P.T., Pratsinis, S.E., 1996. Coagulation and fragmentation: Universal steady-state
8 particle-size distribution. *AIChE Journal* 42(6), 1612-1620.
9 <https://doi.org/10.1002/aic.690420612>
- 10 Su, J., Gu, Z., Li, Y., Feng, S., Xu, X.Y., 2008. An adaptive direct quadrature method of moment
11 for population balance equations. *AIChE Journal* 54(11), 2872-2887.
12 <https://doi.org/10.1002/aic.11599>
- 13 Su, J., Gu, Z., Xu, X.Y., 2009. Advances in numerical methods for the solution of population
14 balance equations for disperse phase systems. *Science in China Series B: Chemistry* 52,
15 1063-1079. <https://doi.org/10.1007/s11426-009-0164-2>
- 16 Tang, Y., Matsoukas, T., 1997. A New Monte Carlo Methods for Simulations of Agglomeration
17 and Grinding. In: *Fine Powder Processing Technology: Proceedings of the Fine Powder*
18 *Processing Conference Sept 1997 Penn State*, pp: 243.
- 19 Tolhurst, T.J., Black, K.S., Shayler, S.A., Mather, S., Black, I., Baker, K., Paterson, D.M., 1999.
20 Measuring the in situ Erosion Shear Stress of Intertidal Sediments with the Cohesive
21 Strength Meter (CSM). *Estuarine, Coastal and Shelf Science* 49(2), 281-294.
22 <https://doi.org/10.1006/ecss.1999.0512>

- 1 Toorman, E. A., 2012. Large-scale modeling of fine-grained sediment transport. Can we do any
2 better?. *Actes des XIII^{ème} Journées Nationales Génie Côtier–Génie Civil (avec*
3 *participation internationale)* 1, 491-502.
- 4 Tran, D., Strom, K., 2017. Suspended clays and silts: Are they independent or dependent
5 fractions when it comes to settling in a turbulent suspension? *Continental Shelf Research*
6 138, 81-94. <https://doi.org/10.1016/j.csr.2017.02.011>
- 7 Tran, D., Strom, K., 2019. Floc sizes and resuspension rates from fresh deposits: Influences of
8 suspended sediment concentration, turbulence, and deposition time. *Estuarine, Coastal and*
9 *Shelf Science* 229, 106397. <https://doi.org/10.1016/j.ecss.2019.106397>
- 10 [Tsai, C. H., Hwang, S. C., 1995. Flocculation of sediment from the Tanshui River estuary.](#)
11 [Marine and freshwater research, 46\(1\), 383-392. https://doi.org/10.1071/MF9950383](#)
- 12 [Verney, R., Lafite, R., Brun-Cottan, J. C., Le Hir, P., 2011. Behaviour of a floc population](#)
13 [during a tidal cycle: Laboratory experiments and numerical modelling. Continental Shelf](#)
14 [Research, 31\(10\), S64-S83. https://doi.org/10.1016/j.csr.2010.02.005](#)
- 15 Walstra, D. J., van Rijn, L. C., Aarninkhof, S. G., 1998. Sand transport at the lower shoreface of
16 the Dutch coast. *Technical Rep. Z*, 2378.
- 17 Wang, C., Yuen, A.C.Y., Chan, Q.N., Chen, T.B.Y., Yang, W., Cheung, S.C.P., Yeoh, G.H.,
18 2020. Characterisation of soot particle size distribution through population balance
19 approach and soot diagnostic techniques for a buoyant non-premixed flame. *Journal of the*
20 *Energy Institute* 93(1), 112-128. <https://doi.org/10.1016/j.joei.2019.04.004>
- 21 Wang, X., Hickernell, F.J., 2000. Randomized halton sequences. *Mathematical and Computer*
22 *Modelling* 32(7-8), 887-899. [https://doi.org/10.1016/S0895-7177\(00\)00178-3](https://doi.org/10.1016/S0895-7177(00)00178-3)

- 1 Wang, X., Sloan, I.H., 2011. Quasi-Monte Carlo methods in financial engineering: An
2 equivalence principle and dimension reduction. *Operations Research* 59, 80-95.
3 <https://doi.org/10.1287/opre.1100.0853>
- 4 Warren, I. R., Bach, H., 1992. MIKE 21: a modelling system for estuaries, coastal waters and
5 seas. *Environmental Software* 7(4), 229-240. [https://doi.org/10.1016/0266-9838\(92\)90006-P](https://doi.org/10.1016/0266-9838(92)90006-P)
- 6 Winterwerp, J. C., 1998. A simple model for turbulence induced flocculation of cohesive
7 sediment. *Journal of Hydraulic Research* 36(3), 309-326.
8 <https://doi.org/10.1080/00221689809498621>
- 9 Winterwerp, J. C., 1999. On the dynamics of high-concentrated mud suspensions.
10 (Ph.D.Dissertation) Delft University of Technology, Netherlands.
- 11 Xu, Z., Zhao, H., Zheng, C., 2014. Fast Monte Carlo simulation for particle coagulation in
12 population balance. *Journal of Aerosol Science* 74, 11-25.
13 <https://doi.org/10.1016/j.jaerosci.2014.03.006>.
- 14 Xu, Z., Zhao, H., Zhao, H., 2017. CFD-population balance Monte Carlo simulation and
15 numerical optimization for flame synthesis of TiO₂ nanoparticles. *Proceedings of the*
16 *Combustion Institute*, 36(1), 1099-1108. <https://doi.org/10.1016/j.proci.2016.07.008>
- 17 Zhang, J.-F., Zhang, Q.-H., 2011. Lattice Boltzmann simulation of the flocculation process of
18 cohesive sediment due to differential settling. *Continental Shelf Research* 31(10), S94-S105.
19 <https://doi.org/10.1016/j.csr.2010.03.009>
- 20 Zhang, J.-F., Zhang, Q.-H., Maa, J.P.Y., Qiao, G.-Q., 2013. Lattice Boltzmann simulation of
21 turbulence-induced flocculation of cohesive sediment. *Ocean Dynamics* 63(9), 1123-1135.
22 <https://doi.org/10.1007/s10236-013-0646-9>

- 1 Zhang, Y., Ren, J., Zhang, W., 2020. Flocculation under the control of shear, concentration and
2 stratification during tidal cycles. *Journal of Hydrology*, 586, 124908.
3 <https://doi.org/10.1016/j.jhydrol.2020.124908>
- 4 Zhao, H., Kruis, F.E., Zheng, C., 2011. Monte Carlo simulation for aggregative mixing of
5 nanoparticles in two-component systems. *Industrial & engineering chemistry research*
6 50(18), 10652-10664. <https://doi.org/10.1021/ie200780q>
- 7 Zhao, H., Zheng, C., 2013. A population balance-Monte Carlo method for particle coagulation in
8 spatially inhomogeneous systems. *Computers & Fluids* 71, 196-207.
9 <https://doi.org/10.1016/j.compfluid.2012.09.025>
- 10 Zhao, K., Vowinckel, B., Hsu, T. J., Köllner, T., Bai, B., Meiburg, E., 2020. An efficient cellular
11 flow model for cohesive particle flocculation in turbulence. *Journal of Fluid Mechanics*,
12 889. <https://doi.org/10.1017/jfm.2020.79>
- 13 Ziff, R.M., McGrady, E.D., 1985. The kinetics of cluster fragmentation and depolymerisation.
14 *Journal of Physics A: Mathematical and General* 18(15), 3027-3037.

15

1 **Figure Captions**

2 Fig.1 The flowchart of the QMC model for cohesive sediment flocculation due to aggregation
3 and fragmentation.

4 Fig.2 Scatter plot of different sampling schemes with each of 1000 points. Top left is the results
5 of pseudorandom (standard MC) approach, top right is Latin hypercube sampling, bottom
6 left is Halton sequence, and bottom right is Sobol' sequence.

7 Fig.3 Time evolution of (a) normalized PSDs and (b) mean sizes for the pure aggregation event
8 with a constant aggregation kernel (Case I)

9 Fig.4 Time evolution of (a) normalized PSDs and (b) mean sizes for the pure fragmentation
10 event with a power law fragmentation kernel. (Case II)

11 Fig.5 Time evolution of (a) normalized PSDs and (b) mean sizes for the combined aggregation
12 and fragmentation events with a constant aggregation kernel and a power law fragmentation
13 kernel. (Case III)

14 Fig.6 The predicted and experimental characteristic sizes and the predicted FSDs for turbulent
15 shear rate $G = 50 \text{ s}^{-1}$ (the first column) and $G = 95 \text{ s}^{-1}$ (the second column) respectively.

16 Fig.7 Comparison between predicted and experimental FSDs of equilibrium for (a) (c)
17 calibration and (b) (d) validation results for suspended kaolinite with different turbulent
18 shear rate.

19 Fig.8 Comparison between predicted and experimental characteristic sizes of equilibrium for
20 suspended kaolinite with different turbulent shear rate.

21 Fig.9 The errors between predicted and experimental results using different QMC sampling
22 schemes for different number of particles.

- 1 Fig.10 The time consumptions of simulation using different QMC sampling schemes for
2 different number of particles. (a) Absolute time consumption; (b) time reductions compare
3 to pseudorandom sequence (standard MC).
- 4 Fig.11 Sensitivity tests for different fragmentation distribution functions in simulation for their (a)
5 characteristic sizes and (b) FSDs.
- 6 Fig.12 Sensitivity tests for different constant and variable fractal dimensions in simulation for
7 their (a) characteristic sizes and (b) FSDs.
- 8 Fig. 13 The change of the mean size and the excess density of flocs with QMC steps.

9

1

Table. 1. The modeling parameters for each experiment, in which λ is the Kolmogorov length scale, D_{\max} is the maximum floc size, and δ is the coefficient in Eq. 32.

Case	N	D_{\max} (μm)	D_p (μm)	nf	$B(D \eta)$
Tran's experiment, $G = 50 \text{ s}^{-1}$	30000	416	5.0	2.2	Binary
Tran's experiment, $G = 95 \text{ s}^{-1}$	30000	258	5.0	2.2	Binary
Maggi's experiment, $G = 10 \text{ s}^{-1}$	30000	316	2.0	$\delta = -0.1$	Binary
Maggi's experiment, $G = 40 \text{ s}^{-1}$	30000	158	2.0	$\delta = -0.1$	Binary
Maggi's experiment, $G = 5 \text{ s}^{-1}$	30000	447	2.0	$\delta = -0.1$	Binary
Maggi's experiment, $G = 20 \text{ s}^{-1}$	30000	223	2.0	$\delta = -0.1$	Binary

2

1

Table. 2. The errors and the time consumptions of different RNG functions with $N = 15000, 30000, 75000,$ and 150000 .

	$N = 15000$	$N = 30000$	$N = 75000$	$N = 150000$
<i>ERROR</i>				
Pseudorandom	0.07341	0.06100	0.05799	0.05525
Sobol'	0.05979	0.05735	0.05428	0.05348
Halton	0.06345	0.05351	0.05162	0.05146
LHS	0.06525	0.06085	0.05616	0.05544
<i>TIME CONSUMPTION</i>				
(s)^a				
Pseudorandom	119	149	271	551
Sobol	118	144	265	530
Halton	119	145	258	510

2 ^a The time consumption of simulation using LHS sequence is not included due to its low efficiency of
3 pretreatments.